Fully Printed Zn-Ag2O Battery Arrays for High Potential Devices

Cher Yeoh

Electrical Engineering and Computer Sciences
University of California at Berkeley

Technical Report No. UCB/EECS-2020-157
http://www2.eecs.berkeley.edu/Pubs/TechRpts/2020/EECS-2020-157.html

August 13, 2020

Contents

Abstract

High voltage miniature devices such as printed thin film transistors and MEMS components used in IoT devices have been demonstrated. However, powering these devices still remains a challenge as common voltage sources such as coin cell batteries have a large device footprint and are not integrated into the device. Printed batteries are an emerging solution to providing on board power supplies due to their small form factor, design flexibility, ease of manufacturing, and low fabrication cost. In this work, a fully printed battery array consisting of six Zn-Ag_2O cells is demonstrated. This work highlights a fully printed battery system that utilizes a vertical geometry fabricated in ambient air with screen printed thick, small-area electrode films to limit the device footprint and maximize areal capacity. Results have shown that the battery arrays can reach a maximum open-circuit voltage of 9V at current densities up to 8 mA cm^{-2} and reach a peak power density of 72mW cm^{-2}. This work demonstrates the potential for printed battery systems to be integrated into miniature devices that require high voltages.

Chapter 1: Introduction

1.1 Motivation

Miniaturization of sensors, actuators, antennas, and common electronic components such as resistors, capacitors, and transistors has been realized. This has allowed us to fabricate miniature devices that can be used in a wide range of applications: from Internet of Things (IoT) devices[1, 2] that can sense and collect data to biological devices such as BioMEMS or wearable health monitoring devices[3, 4, 5]. While advances have been made to scale these devices, further work is needed to design on-board power supplies for these miniaturized devices.[6] Coin cell batteries are most commonly used to power integrated electronic systems; however, they limit the device form factor and constrain the overall device size as they can be orders of magnitude larger than the device and are not integrated into the device. Thus, it is integral to develop a small area and high-energy on-board power supply that can be integrated into the fabrication process of these devices to further allow the miniaturization of these devices. Printed batteries are an emerging solution to providing on board power supplies due to their small form factor, design flexibility, ease of manufacturing, and low fabrication cost. [7, 8]

While printed single cell batteries using various chemistries such as Zn-MnO_2, Zn-Ag_2O, and lithium ion have been demonstrated, [9–15] they are shown to be suitable for only low power devices due to their low operating voltages (< 4V). As we push towards the miniaturization of more and more devices, there will be a demand for higher voltage on-board power supplies. For example, printed organic TFTs used in printed electronic circuits that have been successfully demonstrated are shown to have low mobility, relatively large (10s of μm) channel lengths, and thick (100s of nm) dielectric layers, which requires these organic TFTs to be supplied with a potential (10 – 30 V) to operate. [16] While single cell printed batteries cannot meet these demands, battery arrays can provide sufficient energy and power to drive high voltage devices. By printing an array of cells, the power supply voltage can be increased by connecting cells in series within the array.

1.2 Previous Work

Only a few printed battery arrays of zinc-based systems have been demonstrated, (Gaikwad et al., 2013; Kumar et at., 2017) [16, 17] and further work is needed to incorporate printed batteries with integrated electronics.

Kumar et al. (2017) fabricated stretchable Zn–Ag_2O battery arrays using screen printing. While this work may be suitable for flexible and stretchable devices such as wearable electronics, it is unsuitable to power miniature devices. Their work utilizes a planar geometry which will result in an increase in device footprint internal resistance. In addition, batteries designed with a planar geometry have lower power density and electrode utilization. Gaikwad et al. (2013) demonstrated printed Zn–MnO_2 battery arrays using stencil printing. However, the use of stencil printing makes it difficult to deposit multiple thick electrodes over a large area, which may pose an issue for high throughput processing. Finally, both these systems rely on several non-printed components, such as the separator, that are difficult to incorporate into high throughput assemblies and add to the overall size and cost of the battery.

In this work, a fully printed battery array with small electrode areas that utilizes the Zn-Ag_2O chemistry with a vertical cell geometry is demonstrated. Using screen printing techniques, we were able to fabricate batteries by printing thick Zn electrode films (~120μm) and Ag_2O electrode films (~70μm) on a small area (0.25cm^2). By varying the number of batteries in each array, our battery arrays are able to achieve open-circuit voltages of 3V, 6V, and 9V and can reach power densities up to 72 mW cm^{-2}.

Chapter 2: Battery Architecture

2.1 Substrate

Glass was initially used as the choice for the substrate as previous members of our group have demonstrated printed batteries using a glass substrate.[10] However, the thick (1mm) geometry of the glass substrate, causes the screen mesh to stretch significantly around the edges of the glass substrate while screen printing. This causes the screen to lose tension in certain regions after prolonged use, which may affect the force required to be applied to the screen for a good print. It also damages the screen and introduces the possibility of the screen tearing. In addition, unlike flexible substrates, glass cannot be easily cut to have a specific dimension or geometry. The use of a diamond tip glass cutter or a laser cutter is required; however, even with these tools, it is still difficult to cut the glass substrates to one's desired geometry. For example, both the diamond tip glass cutter and laser cutter require the user to bend the glass along the crack introduced by the cutter, however, user error and other imperfections on the glass may cause the crack to propagate along the wrong direction, resulting in a glass substrate with a different geometry from the cut. Finally, the microscope glass slides available in the lab have a fixed geometry (75mm × 25mm × 1mm and 75mm × 50 mm × 1mm), which means that only glass substrates smaller than the microscope glass slides can be made, which makes it impossible to print larger battery arrays that requires a geometry with an edge larger than 75mm.

To mitigate this issue, a flexible substrate was chosen for this project. Other than being electrically insulating, printable, and chemically compatible with the battery, there are no strict requirements for the surface of the substrates or properties of the substrate. 5mil Kapton (polyimide) film was chosen as the substrate of choice for the battery arrays due to its low cost and high glass transition temperature. More importantly, the Kapton film used is thin, which keeps damage to the screen mesh to a minimum while printing. The geometry of the Kapton substrate can be easily customized using scissors, or a laser cutter. Finally, if further work were to be done, the flexible nature of Kapton allows further investigation of fabricating flexible battery arrays.

2.2 Current Collector

The current collector of a battery allows charge transfers to and from the battery. Ideally, a highly electrically conductive current collector should be used to minimize the internal resistance of the battery. In addition, the current collector must be stable in the presence of the electrolyte; poor chemical stability between the current collector and electrode result in such issues as corrosion or delamination which lead to poor cell performance. Furthermore, when printing, good adhesion must be achieved between the electrode and current collector to prevent the electrode from delaminating from the current collector. Finally, in order to fabricate a fully printed battery array, the current collector must be printable as well. Figure 2.1 provides a summary of the properties of the different current collector materials that were tested.

Advantages	Gold	Silver	Nickel
Printable		✔	✔
Conductivity	✔	✔	
Electrolyte (KOH) Compatibility	✔		✔

Table 2.1: Comparison of the use of gold, silver, and nickel for the current collector material.

Gold was used for previous projects in the group [10]. However, gold was thermally evaporated onto the substrate instead of being printed. Commercially screen printable gold from Creative Materials is available but is expensive and thus not used in this project.

Screen printable nickel (Creative Materials #116-26) was also tested for the choice of current collector material. Despite being fairly stable in the presence of concentrated (8M) KOH solution, the electrical conductivity of the printed nickel films poses an issue. While the specification sheet suggests that the nickel films with have a sheet resistance of 50 Ω/sq at the suggested annealing temperature, experiments were done to determine if varying plasma treatment time and annealing temperature will yield current collectors with minimal resistance. Based on the results, it was observed that printed nickel with sheet resistance less than 10 Ω/sq cannot be achieved. Therefore, nickel is not selected for the choice of current collector material for the batteries.

Screen printable silver (Creative Materials #126-33) was chosen for the material for the current collector. Unlike nickel, the screen printed silver exhibits low resistance. While it is possible for silver to swell and thicken under the presence of concentrated KOH, we have yet to observe any significant cracking or delamination of the silver from the Kapton substrate during the fabrication and testing of the battery arrays that can influence the yield rate and performance of the batteries.

2.3 Electrodes

In a Zn-Ag_2O battery, Zn is the anode and Ag_2O is the cathode. For a printed system, it is crucial to print thick electrode films with high active mass loading to improve the areal capacity of the battery. In addition, thicker Zn electrode films result in greater stability, which can result in higher yield rate and better cell performance; details about the effects of electrode print quality are discussed in chapter 3. The inks are made by mixing the active materials with a binder.

Polyethylene oxide (PEO) binder is used to make Zn and Ag_2O slurries for screen printing. PEO is chosen for the binder for the electrode slurries because it is water soluble, eliminating the need for flammable components from the electrode slurry. Furthermore, PEO is biodegradable,[18] which is a desirable property for disposable primary batteries. Most importantly, by varying the concentration of PEO, the viscosity of the binder can be tuned; details about the effects of viscosity on print quality are discussed in chapter 3.

The binder used for the zinc slurries consists of 4 wt% PEO (M_v = 600, 000) (Sigma #182028) with ~1 wt% PEG 400 in DI water. The binder solution was stirred with a stir bar for 2 hours at 500 rpm to homogenize the solution. The zinc slurry contained 92 wt% Zn (Alfa#10835), 5 wt% ZnO (Sigma #677450), 1 wt% Bi_2O_3 (Alfa #45582), 1 wt% In_2O_3 (Alfa #40394), and 1 wt% binder. The additives (ZnO, Bi_2O_3, In_2O_3) help to suppress hydrogen gas evolution and reduce the rate of zinc corrosion during fabrication and operation. The slurry was hand mixed in a vial using a wooden applicator for about 5 minutes. The Zn electrodes were screen printed on top of the current collectors. After printing, the electrodes are dried at 40 °C to improve electronic conductivity in the electrode.

The binder used for the silver oxide slurries consists of 4.5 wt% PEO (M_v = 600, 000) (Sigma #182028) with ~1 wt% PEG 400 in DI water. The binder solution was stirred with a stir bar for 2 hours at 500 rpm to homogenize the solution. The slurry contained 96 wt% Ag_2O (Strem #93-4743), and 4 wt% binder. The slurry was hand mixed in a vial using a wooden applicator for about 5 minutes. The Ag_2O electrodes were screen printed on top of a separate sheet of current collectors.

The printed square electrodes have an area of 0.25cm^2. The printed Zn electrodes have thicknesses of approximately 120 μm and the printed Ag_2O electrodes have thicknesses of approximately 70 μm.

2.4 Separator, Electrolyte, and Encapsulation Layer

A printable sol–gel using a photopolymerizable polyacrylic acid (PAA) solution previously reported in our group was used as the separator between the anode and the cathode.[19] In addition to being printed, this sol-gel allows a vertical cell structure to be realized, which helps limit the device footprint. The sol-gel separator soaked in 8M KOH electrolyte dissolved with 2.1g ZnO was then encapsulated in a polydimethylsiloxane (PDMS) ring to prevent electrolyte dehydration and ensure suitable ionic conductivity across the separator throughout battery operation.

To prepare the separator, a solution of composed of 0.092g PEO (M_v = 400, 000) (Sigma #372773), 250μL of acrylic acid (Sigma #147230), and ~1 wt% PEG 400 mixed in 3.125mL of 1M KOH was prepared by stirring it for 2 hours at 500rpm to allow the PEO to dissolve. Next, and 0.0185g of photoinitiator (Mw = 224.25) (Sigma #410896) and 0.037g of PEDGE crosslinker (M_n = 250) (Sigma #410195) were added to the solution and stirred for 15min at 650rpm. The solution was then bubbled with nitrogen gas for 10min to deoxygenate the solution. The solution was UV cured using a Spectroline SB-100P UV lamp for 10min. Finally, the separator was soaked in 15μL of 8M KOH electrolyte mixed with 2.1g ZnO for 15min.

The PDMS ring was prepared by mixing the PDMS stock and the curing agent in a 10:1 ratio and then placed in a desiccator for about 15 minutes to remove any bubbles. Next, the PDMS was spin coated on a silicon wafer for 30 seconds at 150 rpm. The PDMS was cured at 150 °C for 10 minutes. Finally, the PDMS was cut to its desired pattern using a laser cutter.

2.5 Interconnects

In order to fabricate battery arrays that can achieve higher potentials, the individual cells are connected in series. After laminating the PDMS ring, silver ink (Creative Materials #126-22) was drop cast on the silver current collectors to connect the anode to the adjacent cathode. 2×1, 2×2, 2×3 array size batteries were fabricated by connecting two, four, and six battery cells, respectively.

2.6 Assembly and Fabrication Process

The fabrication process of the battery arrays is shown in figure 2.1 Starting with an untreated Kapton substrate, silver current collectors are deposited using screen printing. A second substrate with the same current collector pattern is prepared. We then screen-print zinc and Ag2O electrodes onto their respective current collector substrates. Spin-coated polydimethylsiloxane (PDMS) encapsulation rings are then laminated to the surface of the zinc electrode array substrate. The PDMS encapsulation layer has shown to be printed in other works. [20] In order to connect the anode of one battery to the cathode of the adjacent cell, silver interconnects were added to the design. These interconnects were deposited using drop casting to connect the batteries in the array in series, before laminating together the two separate zinc and silver oxide electrode arrays together. The interconnects were drop cast between two adjacent PDMS ring edges, separating two adjacent zinc electrodes. Afterwards, the sol-gel soaked in KOH electrolyte was placed on top of each zinc electrode. Finally, the array of Ag2O electrodes were laminated together by visually aligning the printed alignment marks on the zinc and silver oxide substrates. A 3D schematic of the printed 2 ×3 Zn-Ag_2O battery array is shown in figure 2.2. The batteries are connected in a ‘U’ shaped fashion, each separated with a distance of 9mm.

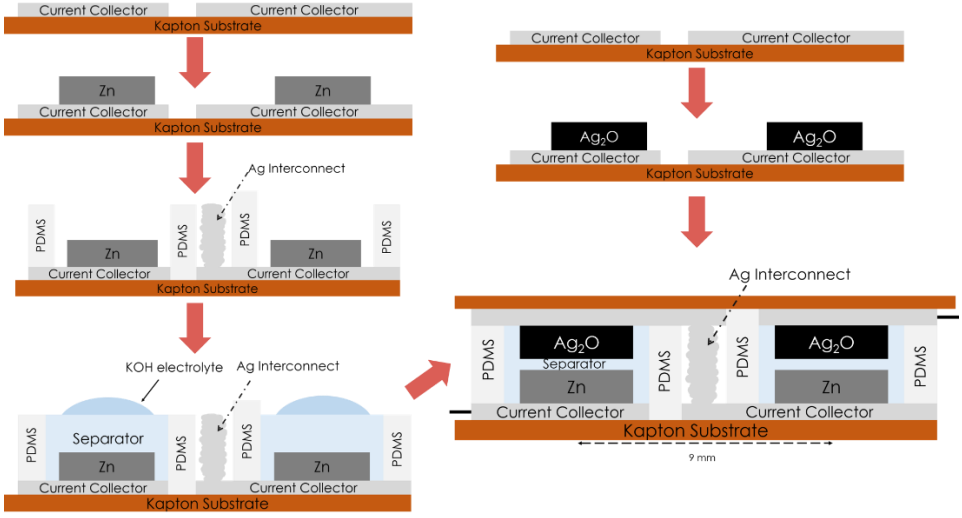

Figure 2.1: Fabrication process of a printed Zn-Ag_2O battery array (cross sectional view).

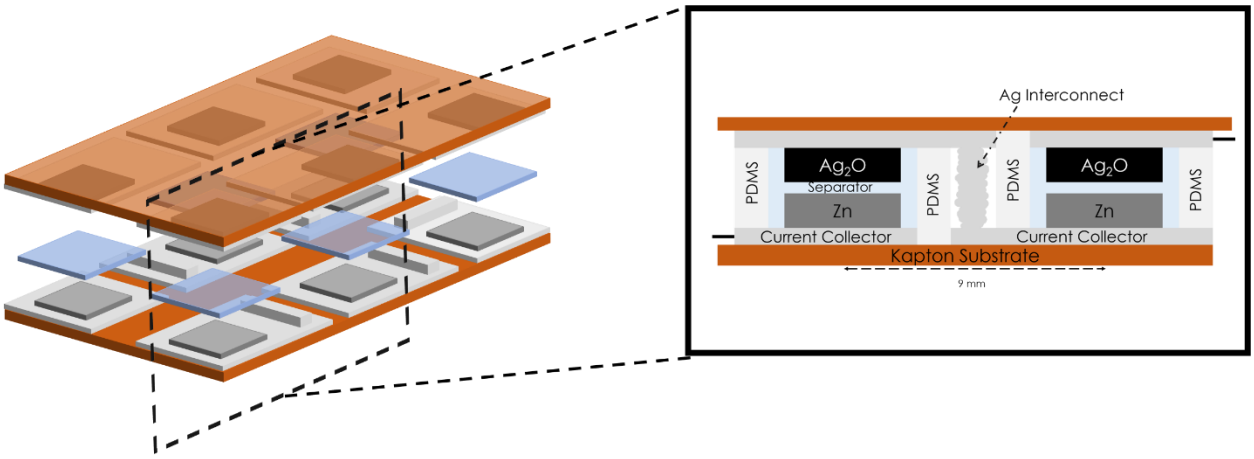

Figure 2.2: Schematic of a printed 2×3 Zn-Ag_2O battery array.

Chapter 3: Ink Development and Electrode Print Quality

3.1 Importance of Electrode Print Quality

Because both the Zn and Ag_2O electrodes are the same size (0.25 cm^2), Ag_2O is the limiting electrode and thus the mass loading of the Ag_2O dictates the cell capacity. In addition, during fabrication and operation of the battery, Zn corrosion issues may occur, which may cause stability issues; therefore, the Zn electrode is the "limiting stability" electrode. It was observed that thin (< 35μm), rough Zn films with pinholes suffer from significant corrosion issues because a larger area of the Zn electrode surface is exposed. Visible ZnO precipitates were formed on thin Zn electrodes during the fabrication of the battery which may impede ion transfer. This leads to poor cell performance and low yield rate. Figure 3.1 shows the formation of ZnO precipitates on the surface of a thin, porous Zn electrode after the sol-gel separator was laminated on the Zn surface.

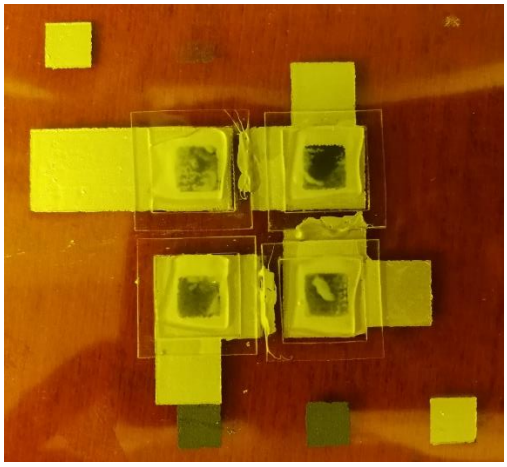

Figure 3.1: Formation of (white) ZnO precipitates on Zn electrodes with poor print quality

The environment the Zn electrode is in dictates the corrosion rate per unit area of the Zn on the surface of the printed electrode film. Changing the electrolyte and separator composition may help reduce the corrosion rate per unit area but may result in poorer charge transfer. Because the corrosion rate per unit area of the Zn electrode is constant under a controlled, unchanging environment, printing thicker, smooth, and non-porous Zn electrode films can help mitigate corrosion and stability issues. Thus, it is crucial to print thick, smooth, and nonporous Zn and Ag2O electrode films to increase the stability and capacity of the battery.

Raj Kumar (PhD, summer 2019) in our group demonstrated that batteries fabricated using stencil printing with smooth Zn electrode thickness of approximately 100 μm free of pinholes will not cause any significant corrosion issues and are fairly stable during the operation of the battery.[10] Therefore, to fabricate screen printed batteries with high yield rate and good performance, I aimed to print Zn electrode films thicker than 100μm.

3.2 Binder Viscosity

The ink must be tuned to the appropriate viscosity to ensure good transfer of the pattern through the screen mesh. For screen printing, the viscosity of the ink must be between somewhere 500 cP – 5000 cP.[4] At higher viscosities, inks tend to clog the mesh and impede ink deposition. At lower viscosity, the ink may spread out, resulting in poor feature definition. In both cases, they result in thin films with printing defects that can impact battery capacity and yield rate. It is important for successful printing that the ink be "shear thinning," i.e. that the viscosity goes down with increasing shear rate as shown in figure 3.2. Figure 3.2 shows a plot of shear rate against viscosity for PEO binder at various concentrations (by weight) in water. In general, as the PEO concentration of the binder increases, the viscosity of the binder increases.

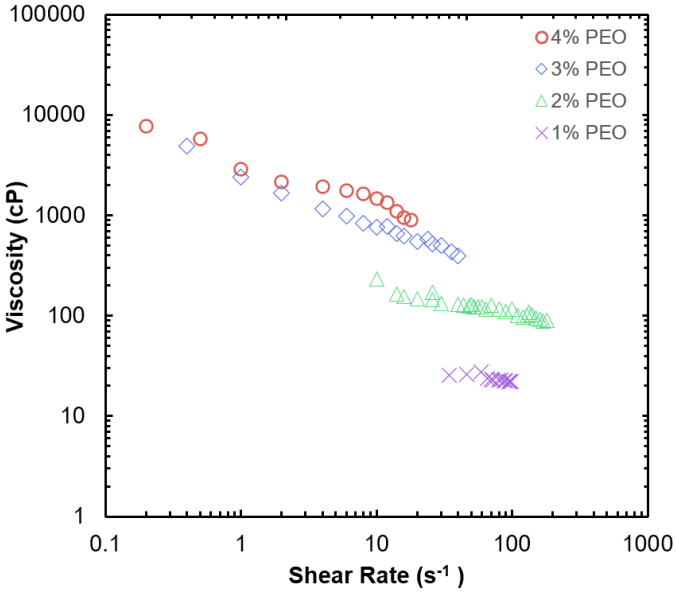

Figure 3.2: Plot of shear rate against viscosity for PEO binder at various concentrations (by weight) in water

Different print qualities were obtained depending on the binder concentration used. Optical microscope images of printed Ag_2O film using binder concentrations of 1-4% are found in figure 3.3a-d. Notable defects on the lower concentrations were large quantities of pinholes as well as very rough films. However, the 4.5% PEO binder yielded a relatively uniform single layer print and was used for all future Ag_2O ink preparations. A similar trend was also observed for printed zinc electrodes. For zinc, 4% PEO binder resulted in the best print and was used for this project. Visible pinholes may be observed in figures 3.3a-d and may pose a problem to the yield rate and performance of the battery however, the pinholes may be covered up by printing multiple passes (more details in chapter 3.4).

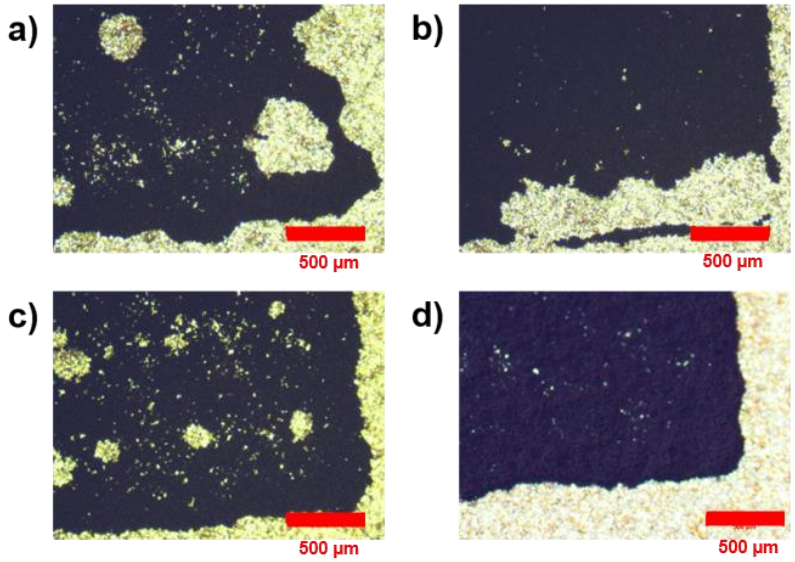

Figure 3.4: Optical microscope image of printed Ag2O film using a) 1% PEO binder, b) 2% PEO binder, c) 3% PEO binder, and d) 4% PEO binder. The scale bar for the micrographs represents 500 µm

3.3 Print Quality vs. Mass Loading

In addition to tuning binder viscosity, print quality of the electrode films may be tuned by varying the mass of the active material. As shown in figure 3.5, it can be observed that printed films with 96 wt% Ag_2O and 4% binder solution results in film thicknesses of around 50 µm with fewer pinholes and print defects compared to inks with lower mass loadings. Similar experiments were done for Zn electrodes and it was found that the optimal mass loading for Zn consists for 1% binder with 99 wt% of active material and 1% binder solution. Film thicknesses of around 50 µm were also achieved for Zn electrodes in a single pass.

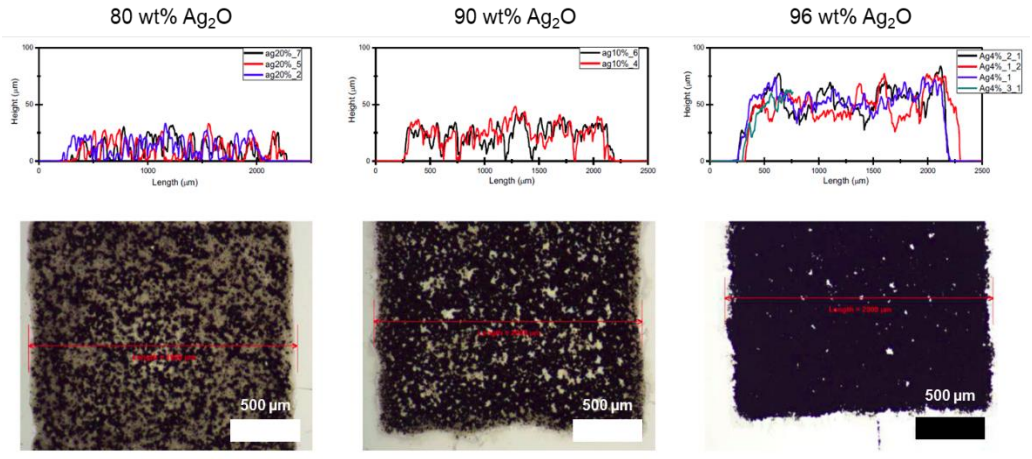

Figure 3.5: Print quality of Ag_2O electrode films at varying mass loading. The scale bar for the micrographs represents 500 µm. Legends represent different trials of the same experiment.

3.4 Print Quality vs. Print Passes

The average thicknesses that can be achieved in one print passes are around 50 µm for both Zn and Ag_2O electrodes. Batteries fabricated with film thicknesses of approximately 50 µm have a yield rate of approximately 70% – 80%. The yield rate can get even worse as the screen degrades over time, as screen degradation results in slightly thinner film and rougher film; more details are discussed in chapter 3.5. It is crucial for batteries fabricated in an array to have a high yield rate because a failure in only one of the multiple batteries in the array causes the whole battery array to be unable to reach its intended open circuit voltage. Therefore, to combat the yield rate issues, multiple print passes were done to increase the thickness of the electrodes. Printing thicker Zn electrodes is prioritized since Zn is the limiting stability electrode, which dictates whether the battery will fail. Multiple print passes were also done while printing Ag_2O films, as thicker and smoother Ag_2O films can increase the battery capacity.

By printing over the same layer multiple times, thicker, smoother, and less porous films are formed. Figure 3.5 shows the profilometry of zinc and silver oxide films, depending on the number of print passes used to prepare the electrode. In order to deposit thicker electrodes, multiple screen-printing passes were used, letting each printed film dry at room temperature for 10 minutes before depositing the next. By depositing multiple layers of the same material, pinholes formed from layer one were filled in, as well as yielding thicker electrodes films, with an average thickness of 120µm for the zinc electrodes, and 70um for the Ag2O electrodes. For Zn films, it is shown that the thickness of the film significantly improves with the number of print passes. The average thickness for Zn films after one, two, and three print passes are approximately 50µm, 80µm, and 120 µm, respectively. For Ag2O films, while the thickness doesn't seem to increase significantly, pinholes were filled up as shown in figure 3.6. The average thickness for Ag2O films after one, two, and three print passes are approximately 50µm, 60µm, and 70µm, respectively. The battery arrays are fabricated using electrode films with three print passes.

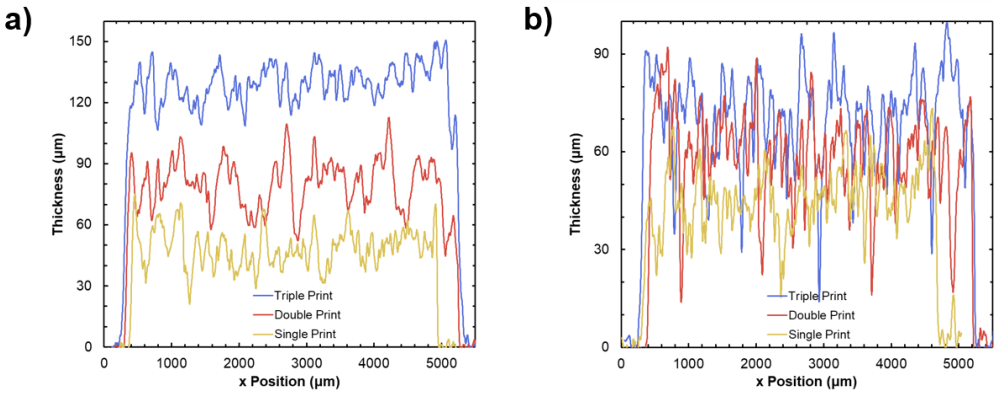

Figure 3.5: a) Profilometry measurements for screen printed Zn films with varying number of print passes. b) Profilometry measurements for screen printed Ag_2O films with varying number of print passes.

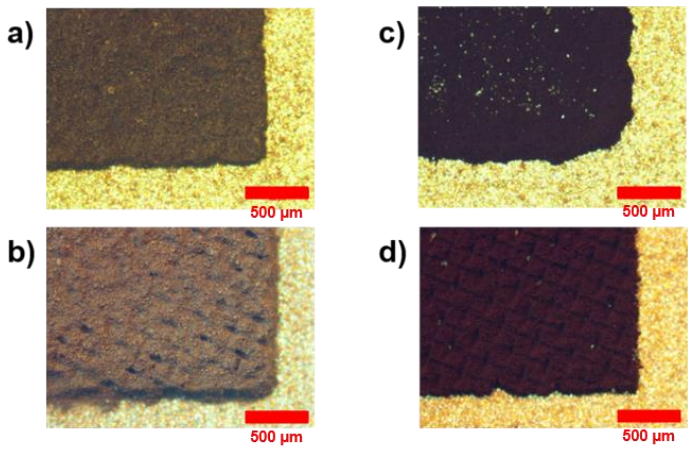

Figure 3.6: Optical microscope images of a) a single print, b) a triple printed Zn electrode. Optical microscope images of c) a single print, and d) a triple printed Ag_2O electrode. The scale bar for the micrographs represents 500 µm

3.5 Print Quality Degradation

It was observed that the print quality is hugely dependent on the quality of the screen. Poor maintenance of the screen after multiple uses may clog the screen and result in poorer ink transfer, resulting in rougher and thinner films with increased defects such as pinholes and film roughness. As illustrated in figure 3.7, the average film thickness after a single print pass decreased from around 50 µm to 38 µm for Zn electrodes films and 50 µm to 33 µm for Ag_2O electrode films after using the screen for about half a year. As a result of having thinner films, the total mass loading has reduced as well; a numerical measurement for the mass loading may be determined by computing the area under the profilometry curve. The area under the profilometry curve after one print pass decreased from 1.78e6 μm^2 to 1.67e6 μm^2 and 2.42e6 μm^2 to 1.33e6 μm^2 for Zn and Ag_2O electrode films, respectively. Therefore, careful monitoring and cleaning of the screen is required for transfer of ink and good print quality. If it is observed that print quality has reduced significantly and affects the yield rate and performance of the battery, the screen will need to be replaced.

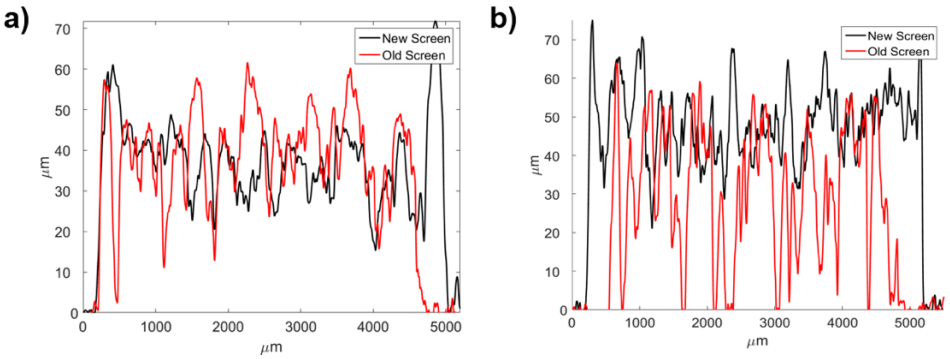

Figure 3.7: a) Profilometry measurements for screen printed Zn films after a single pass with a new screen and old screen. b) Profilometry measurements for screen printed Ag_2O films after a single pass with a new screen and old screen.

Chapter 4: Battery Performance

4.1 Battery Testing

Experiments were done using the Biologic BCS-810 battery tester. Prior to testing, an initialization step was done at 0.25 mA cm^{-2} for 1 min. For polarization measurements, the battery was discharged at a fixed current density (1 mA cm^{-2} – 8 mA cm^{-2}) for 2 min. For constant current discharge measurements, the battery was discharged at a 0.2 mA cm^{-2}.

4.2 Single Cell Performance

To evaluate the performance of the screen printed batteries, single cell batteries were first fabricated using screen printing methods and its performance was compared batteries fabricated using stencil printing. Figure 4.1 shows the polarization data of the screen printed cells. Cells were fabricated with 25mm^2 electrode size and discharged at current densities ranging from 1mA cm^{-2} to 12 mA $cm^{-2.}$ It was observed that the operating voltage decays slightly with increasing current density but maintains an operating potential above 1.4 V at current densities up to 12 mA cm-2 and has maximum power density of 17 mW cm^{-2}, which matches the results from Raj's work on stencil printed single cell batteries. The battery was also discharged at a constant current to determine its total areal capacity. Figure 4.2 displays the constant current discharge profile of the printed battery, which shows that the screen printed cells can reach areal capacities of about 1.2 mAh cm^{-2}. In addition, it is shown that the standard deviations of the operating voltage and power densities are less than 50 mV and 200 mW cm^{-2}, respectively, which demonstrates the reproducibility of the screen printed batteries.

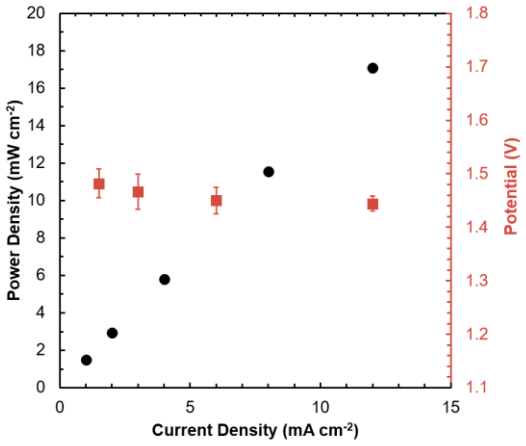

Figure 4.1: Polarization data for screen printed single cell Zn-Ag_2O battery up to 12 mA cm^{-2}.

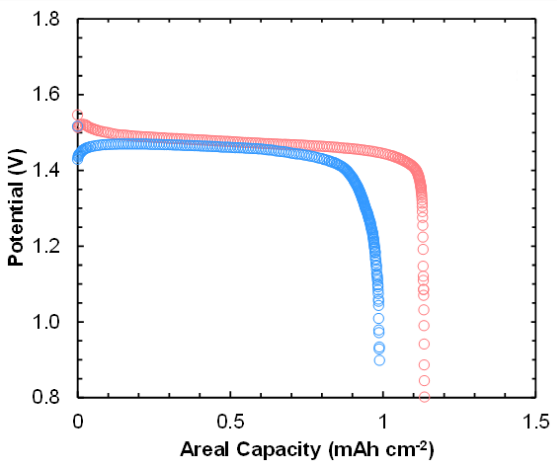

Figure 4.2: Discharge profiles for two different screen printed single cell Zn-Ag_2O batteries at 2mA cm^{-2}

4.3 Array Performance

After screen printed cell performance was established, screen printed battery arrays were demonstrated. Using drop cast Ag interconnects between cells, batteries with array sizes of 2×1, 2×2, and 2×3 with electrode sizes of 25mm^2 were fabricated. As shown in Figure 5.3, the operating voltages were shown to scale to an average about 2.95V, 6.08 V, and 9.00 V for 2×1, 2×2, 2×3 array size batteries, respectively, which shows that there is little to no resistance introduced from the silver interconnects. It can be observed that the batteries maintain an operating potential above 2.9 V, 5.9 V, and 8.9 V at current densities up to 8 mA cm-2, and have maximum power density of 17 mW cm^{-2}, 23 mW cm^{-2}, 72 mW cm^{-2} for 2×1, 2×2, 2×3 array size batteries, respectively. Like single cell batteries, the operating voltage decays slightly with increasing current density and a small standard deviation for operating voltage (< 50 mV) and power densities (< 370 mV cm^{-2}) were observed.

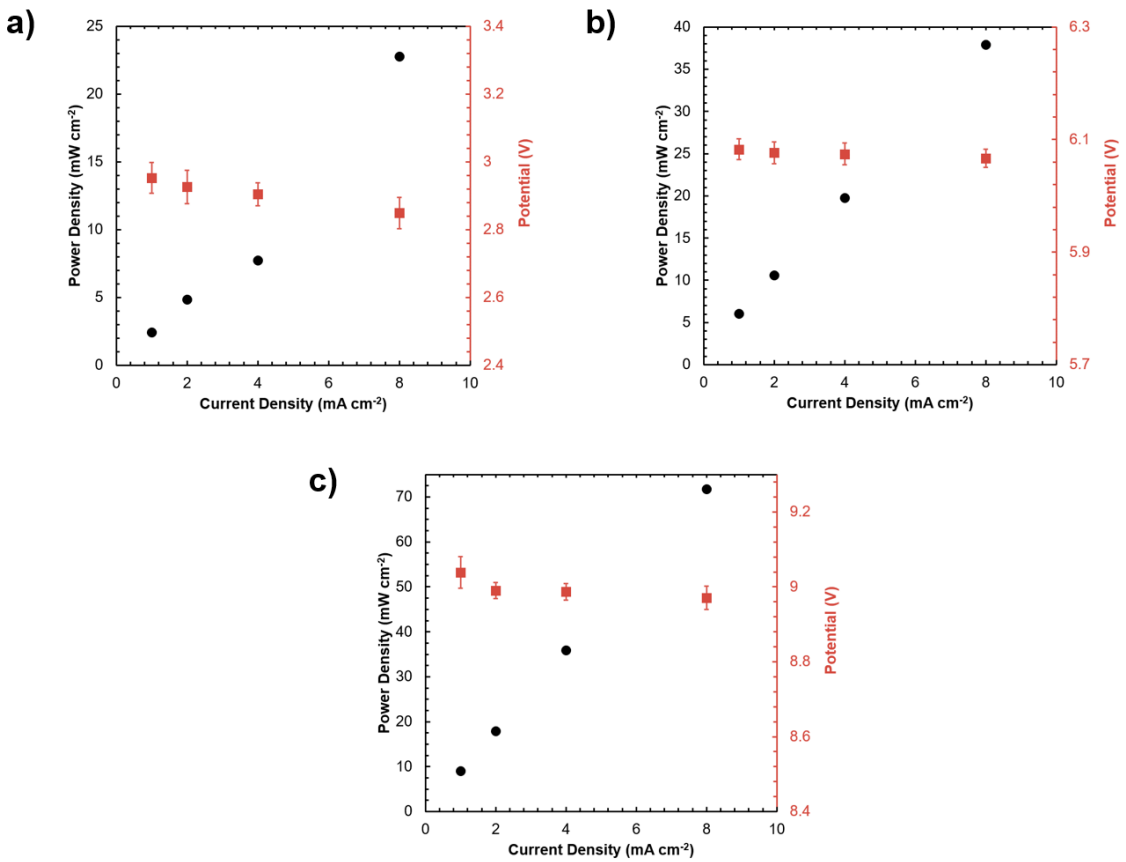

Figure 4.1: Polarization data for screen printed Zn-Ag_2O battery arrays up to 8 mA cm^{-2} for a) 2×1 arrays, b) 2×2, arrays, and c) 2×3 arrays.

Chapter 5: Conclusion

In summary, we developed a fully printed battery array capable of achieving open circuit voltages at 1.5V, 3V, 6V, and 9V. By utilizing the vertical cell geometry and small footprint (0.25 cm^2) electrodes, the Zn – Ag_2O battery arrays we designed can be easily integrated into existing process flows. Using screen printing techniques, the current collectors, along with the anode and cathode electrodes are printed. By tuning the viscosity and mass loadings of the electrode slurries, ink suitable for screen printing were developed. Multiple print passes were done to increase the overall thickness of the film and improve print quality, such as reducing pinholes and surface roughness, to improve battery yield rate and capacity. With three print passes, Zn electrodes with average thicknesses of 120μm and Ag_2O electrodes with average thicknesses of 70μm were achieved. Battery arrays consisting up to six cells were fabricated and were able to maintain an operating voltage of 8.9 V at current densities up to 8 mA cm^{-2} and reach a peak power density of 72mW cm^{-2}. Our work demonstrates the potential for printed battery systems to be integrated into miniature devices that require high potentials, such as IoT devices that can sense and collect data, and biological devices such as BioMEMS or wearable health monitoring devices.

Bibliography

[1] B. Warneke, M. Last, B. Liebowitz, K. S. J. Pister, *Computer (Long. Beach. Calif).* **2001**, *34*, 44.
[2] J. M. Kahn, R. H. Katz, K. S. J. Pister, *J. Commun. Networks* **2000**, *2*, 188.
[3] Y. Khan, D. Han, J. Ting, M. Ahmed, R. Nagisetty, A. C. Arias, *IEEE Access* **2019**, 7, 128114.

[4] Y. Khan, D. Han, A. Pierre, J. Ting, X. Wang, C. M. Lochner, G. Bovo, N. Yaacobi-Gross, C. Newsome, R. Wilson, A. C. Arias, *Proc. Natl. Acad. Sci. USA* **2018**, *115*, E11015

[5] M. E. Payne, A. Zamarayeva, V. I. Pister, N. A. D. Yamamoto, A. C. Arias, *Sci. Rep.* **2019**, 9, 13720.

[6] M. R. Lukatskaya, B. Dunn, Y. Gogotsi, *Nat. Commun.* **2016**, 7, 1.

[7] Y. Khan, M. Garg, Q. Gui, M. Schadt, A. Gaikwad, D. Han, N. A. D. Yamamoto, P. Hart, R. Welte, W. Wilson, S. Czarnecki, M. Poliks, Z. Jin, K. Ghose, F. Egitto, J. Turner, A. C. Arias, *Adv. Funct. Mater.* **2016**, 26, 8764.

[8] R. E. Sousa, C. M. Costa, S. Lanceros-Mendez, *ChemSusChem* **2015**, 8, 3539

[9] A.M. Zamarayeva, A. Jegraj, A. Toor, V. I. Pister, C. Chang, A. Chou, J. Evans, A. C. Arias, *Energy Technology*, **2019**, 1901165**.**

[10] R. Kumar, K. M. Johnson, N. X. Williams, V. Subramanian, *Adv. Energy Mater.* **2019**, 9, 1803645

[11] M. Koo, K.-I. Park, S. H. Lee, M. Suh, D. Y. Jeon, J. W. Choi, K. Kang, K. J. Lee, *Nano Lett.* **2012**, *12*, 4810

[12] S. Berchmans, A. J. Bandodkar, W. Jia, J. Ramírez, Y. S. Meng, J. Wang, J. *Mater. Chem. A* **2014**, *2*, 15788.

[13] A. M. Gaikwad, G. L. Whiting, D. A. Steingart, A. C. Arias, *Adv. Mater.* **2011**, *23*, 3251.

[14] A. M. Gaikwad, A. M. Zamarayeva, J. Rousseau, H. Chu, I. Derin, D. A. Steingart, *Adv. Mater.* **2012**, *24*, 5071.

[15] X. Wang, S. Zheng, F. Zhou, J. Qin, X. Shi, S. Wang, C. Sun, X. Bao, Z.-S. Wu, *Natl Sci. Rev.* **2019**, *7*, 64

[16] A. M. Gaikwad , D. A. Steingart , T. N. Ng , D. E. Schwartz , G. L. Whiting , *Appl. Phys. Lett.* **2013**, *102*, 233302 .

[17] R. Kumar, J. Shin, L. Yin, J. You, Y. S. Meng, J. Wang, *Adv. Energy Mater.* **2017**, *7*, 1602096.

[18] Reed, A. M.; Gilding, D. K. *Polymer* **1981**, *22*, 499.

[19] K. Braam, V. Subramanian, *Adv. Mater.* **2015**, *27*, 689

[20] D. B. Kolesky, R. L. Truby, A. S. Gladman, T. A. Busbee, K. A. Homan, J. A. Lewis, *Adv. Mater.* **2014**, *26*, 3124.